



Aalborg Universitet

AALBORG UNIVERSITY
DENMARK

Evaluation of predicted patellofemoral joint kinematics with a moving-axis joint model

Dzialo, Christine Mary; Pedersen, Peter Heide; Jensen, Kenneth Krogh ; de Zee, Mark; Andersen, Michael Skipper

Published in:
Medical Engineering & Physics

DOI (link to publication from Publisher):
[10.1016/j.medengphy.2019.08.001](https://doi.org/10.1016/j.medengphy.2019.08.001)

Creative Commons License
CC BY-NC-ND 4.0

Publication date:
2019

Document Version
Accepted author manuscript, peer reviewed version

[Link to publication from Aalborg University](#)

Citation for published version (APA):
Dzialo, C. M., Pedersen, P. H., Jensen, K. K., de Zee, M., & Andersen, M. S. (2019). Evaluation of predicted patellofemoral joint kinematics with a moving-axis joint model. *Medical Engineering & Physics*, 73, 85-91. <https://doi.org/10.1016/j.medengphy.2019.08.001>

General rights

Copyright and moral rights for the publications made accessible in the public portal are retained by the authors and/or other copyright owners and it is a condition of accessing publications that users recognise and abide by the legal requirements associated with these rights.

- ? Users may download and print one copy of any publication from the public portal for the purpose of private study or research.
- ? You may not further distribute the material or use it for any profit-making activity or commercial gain
- ? You may freely distribute the URL identifying the publication in the public portal ?

Take down policy

If you believe that this document breaches copyright please contact us at vbn@aub.aau.dk providing details, and we will remove access to the work immediately and investigate your claim.

1 **Evaluation of predicted patellofemoral joint kinematics with a moving-axis joint model**

2

3 C M Dzialo^{1,2*}, P H Pedersen³, K K Jensen⁴, M de Zee⁵, M S Andersen²

4

5 ¹*AnyBody Technology, A/S Niels Jernes Vej 10, DK 9220 Aalborg, Denmark*

6 ¹*Department of Materials and Production, Aalborg University, Fibigerstræde 16, DK-9220 Aalborg,*

7 *Denmark*

8 ²*Department of Orthopedic Surgery, Aalborg University Hospital, Hobrovej 18-22, DK-9000*

9 *Aalborg, Denmark*

10 ³*Department of Radiology, Aalborg University Hospital, Hobrovej 18-22, DK-9000 Aalborg,*

11 *Denmark*

12 ⁴*Department of Health Science and Technology, Sport Sciences, Aalborg University, Fredrik Bajers*

13 *Vej 7D, DK-9220 Aalborg*

14

15

16 Submitted to *Medical Engineering and Physics* as a Short Communication, 12/2018

17 Revised and resubmitted to *Medical Engineering and Physics* as a Technical Note, 07/2019

18

19 *Keywords:* Patellofemoral joint, secondary joint kinematics, magnetic resonance imaging,

20 musculoskeletal knee model, EOS Imaging

21 *Word count* (Introduction through Discussion): 2334/3500

22

23 *Corresponding author:

24 Christine Dzialo

25 Department of Materials and Production, Aalborg University, Fibigerstræde 16, DK-9220 Aalborg,

26 Denmark

27 Tel. +45 42 48 98 90

28 E-mail: christinedzialo@gmail.com or cmd@anybodytech.com

29 **Abstract**

30 The main objectives of this study were to expand the moving-axis joint model concept to the
31 patellofemoral joint and evaluate the patellar motion against experimental patellofemoral kinematics.
32 The experimental data was obtained through 2D-to-3D bone reconstruction of EOS images and
33 segmented MRI data utilizing an iterative closest point optimization technique. Six knee model
34 variations were developed using the AnyBody Modeling System and subject-specific bone
35 geometries. These models consisted of various combinations of tibiofemoral (hinge, moving-axis, and
36 interpolated) and patellofemoral (hinge and moving-axis) joint types. The newly introduced
37 interpolated tibiofemoral joint is calibrated from the five EOS quasi-static lunge positions. The
38 patellofemoral axis of the hinge model was defined by performing surface fits to the patellofemoral
39 contact area; and the moving-axis model was defined based upon the position of the patellofemoral
40 joint at 0° and 90° tibiofemoral-flexion. In between these angles, the patellofemoral axis moved
41 linearly as a function of tibiofemoral-flexion, while outside these angles, the axis remained fixed.
42 When using a moving-axis tibiofemoral joint, a hinge patellofemoral joint offers (-5.12 ± 1.23 mm,
43 5.81 ± 0.97 mm, $14.98 \pm 2.30^\circ$, $-4.35 \pm 1.95^\circ$) mean differences (compared to EOS) while a moving-
44 axis patellofemoral model provides (-2.69 ± 1.04 mm, 1.13 ± 0.80 mm, $12.63 \pm 2.03^\circ$, $1.74 \pm 1.46^\circ$) in
45 terms of lateral-shift, superior translation, patellofemoral-flexion, and patellar-rotation respectively.
46 Furthermore, the model predictive capabilities increased as a direct result of adding more calibrated
47 positions to the tibiofemoral model (hinge-1, moving-axis-2, and interpolated-5). Overall, a novel
48 subject-specific moving-axis patellofemoral model has been established; that produces realistic
49 patellar motion and is computationally fast enough for clinical applications.

50

51

52

53

54

55

56

57

58

59

60

61

62

63

64

65

66

67

68 **1. Introduction**

69 The patellofemoral (PF) joint contains the body's largest sesamoid bone, the patella, nestled in the
70 femoral trochlear groove. The patella acts as a lever arm to translate force from the quadriceps muscle
71 across the tibiofemoral (TF) joint, while also serving as a bony shield to protect the tibiofemoral joint
72 [1]. Dysfunction and mal-tracking often arise when the homeostasis of a joint is compromised [2–5],
73 for example: increased patellar tilt [6,7], a more laterally positioned tibial tuberosity [8], abnormal
74 “screw-home” rotation of the tibiofemoral joint [9], and hip muscle weakness [10] especially in the
75 female population [11] may lead to anterior knee pain during activities of daily living. In addition,
76 correlations exist between the patellofemoral morphology and resulting kinematics [7,12] so it is
77 important that subject-specific morphology is captured when constructing musculoskeletal joint
78 models.

79 Musculoskeletal modeling is a non-invasive computational tool used to better understand what occurs
80 in the body internally as a result of external loads and movements. The patellofemoral joint is often
81 excluded from pure kinematic models [13]; however when it is included, it is frequently modeled as a
82 1 degree-of-freedom hinge joint with an additional rigid patella tendon [14–22] which may not
83 provide realistic joint kinematics. In hopes of achieving more realistic joint kinematics, researchers
84 have included a 6 degrees-of-freedom patellofemoral joint utilizing multi-body contact models
85 [17,23–31]. The main advantage of these models is that they can capture contact and ligaments forces;
86 however, they may be too computationally slow for clinical applications.

87 The main objective of this study, therefore, was to establish a more computationally fast
88 patellofemoral model capable of predicting subject-specific patellar motion when using motion
89 capture input, while also avoiding error from skin artifact movement, for future use in the clinical
90 setting. This model applies the concepts established in the moving-axis tibiofemoral joint model [32]
91 to the patellofemoral joint. In a moving-axis joint applied to the knee (patellofemoral or tibiofemoral),
92 the articulation is model such that the joint axis moves linearly back and forth between two known
93 positions, as a function of tibiofemoral flexion. The proposed model was evaluated against the patellar

94 positions extracted from a series of bi-planar EOS x-rays, which has an accuracy of 0.95 ± 0.55 mm
95 [32].

96

97 **2. Methods**

98 *Data Collection*

99 Preexisting imaging data [33], approved by the Scientific Ethical Committee for the Region of
100 Nordjylland, was utilized in this study. This dataset consisted of lower limb Magnetic Resonance
101 Image (MRI) acquisitions (T1W-LAVA-XV-IDEAL COR, 1.6 mm slice thickness, 0 mm gap
102 thickness) of ten healthy male subjects (age 33 ± 10 years, body mass 79 ± 11 kg, height 1.82 ± 0.07
103 m) and five low dose radiation orthogonal x-rays (EOSTM) of the loaded knee joint at roughly 0° , 20° ,
104 45° , 60° , and 90° tibiofemoral-flexion during a quasi-static lunge.

105 *Patella segmentation and registration*

106 Bone surface geometries and contours of the patella were manually segmented from the lower limb
107 MRIs and biplane EOS images respectively, using Mimics Research 19.0 (Materialise, Leuven,
108 Belgium). Custom MATLAB (The Mathworks Inc., Natick, MA, USA) code was used to manually
109 transform the 3D bone geometry and its' projected contours to roughly match the segmented biplanar
110 contours. Then, an iterative closest point approach was employed to minimize the least-square
111 difference between the contour sets. EOS reconstructions of the 3D patella positions and orientations
112 for each set of EOS images were then read into the AnyBody Modeling System (AMS v 7.1,
113 AnyBody Technology A/S, Denmark) to calculate translations and rotations of the patellofemoral
114 joint.

115 *Joint coordinate system (CS) and kinematic measures*

116 For EOS data and all models, the patella anatomical CS origin was defined at the center of the
117 outermost superior, inferior, medial, and lateral points. Each of these points were determined by first
118 manually selecting the general location in 3-Matic Research 11.0 (Materialise, Leuven, Belgium),

119 exporting this surface as a STL, and then taking an average of the STL cluster in MATLAB. The
120 orientation was determined by (1) creating a temporary flexion axis running between the medial-
121 lateral points, (2) defining the long axis (directed superiorly) between the superior-inferior points, (3)
122 the anterior-posterior axis was defined as the cross product between (1) and (2), and finally the real
123 medial-lateral axis was defined as the cross product between (2) and (3) [34–37]. We defined the
124 patellofemoral joint in terms of a femoral and patella fixed-body axis with a perpendicular floating
125 axis (Figure 1), adapted from the ISB standards of the tibiofemoral joint [35,38,39]. The femoral
126 anatomical axis was defined with the y-axis running from the center point between the two
127 epicondyles to the hip joint center. The z-axis was defined orthogonal to the y-axis and pointing
128 towards the lateral epicondyle. Finally, the x-axis is defined as the cross product between the y-axis
129 and z-axis pointing anteriorly [33,40–43]. The tibiofemoral joint was defined using ISB standards [38]
130 and is discussed in detail in Dzialo et al. (2018).

131 *Knee Model Development*

132 Six knee models were created using combinations of tibiofemoral and patellofemoral joint types
133 (Supplementary Table 1). These joint types include: two previously established tibiofemoral joint
134 models (hinge and moving-axis) [33], one new tibiofemoral joint (Interpolation-INT), and two new
135 patellofemoral joints (hinge and moving-axis). In each knee model, the patellar tendon is defined as a
136 non-deformable element, connecting the patella to the tibia tuberosity.

137 Hinge: The tibiofemoral hinge joint axis was defined as a line running from the medial to lateral
138 femoral epicondyles from the EOS_0 reconstruction pose [33]. To determine the patellofemoral hinge
139 joint axis, we first applied a least-squares cylindrical fitting function using MATLAB to the medial
140 and lateral surfaces of the femoral trochlear groove [44,45] to find the respective centers. The
141 patellofemoral hinge joint axis was then defined by a line connecting these centers (Figure 2.a).

142 Moving-Axis (MA): The tibiofemoral MA joint model was taken directly from Dzialo et al. (2018).
143 The patellofemoral MA model was calibrated from the position and orientation of the patellofemoral
144 joint in the 0° and 90° EOS reconstructions. We fit four cylinders to femoral trochlear groove surface

145 selections (Figure 2.b-c), which were based on selections made by Bowes et al. 2015 [44,45] and
146 discussed in the Hinge section above, based on where the patella contacts the femur when the
147 tibiofemoral joint is in full extension (EOS-0), and in roughly 90° flexion (EOS-90). The facet centers
148 from medial and lateral cylinder fits in extension (EFC) and flexion (FFC) were connected to define
149 two axes (Figure 2.b-c). During hyperextension of the tibiofemoral joint, we assumed that the
150 patellofemoral joint rotates about the EFC axis. For TF-flexion angles greater than the EOS 90°
151 reconstruction, rotation occurs about the FFC axis. We assumed angles within these limits will move
152 linearly as a function of TF-flexion between the patellofemoral EFC to FFC axes.

153 Interpolation (INT): Due to the correlation between patellofemoral and tibiofemoral joint kinematics
154 during weighted knee flexion, and the fact that the patellofemoral moving-axis is expressed as a
155 function of the tibiofemoral flexion angle, the error present in the tibiofemoral joint may influence the
156 model's predictability of the patellofemoral kinematics. This is especially the case in terms of PF-
157 flexion, tilt, anterior-posterior (AP), and medial-lateral (ML) translations [46]. The Interpolation
158 tibiofemoral model was simulated by applying a piecewise linear function, between the exact
159 measured points from the tibiofemoral EOS reconstructions. With this, the only model error left
160 would be within the patellofemoral model when comparing against the EOS experimental data.

161 *Model Evaluation and Statistics*

162 Patellofemoral kinematics were extracted from each EOS reconstruction (0°, 20°, 45°, 60°, and 90°).
163 Corresponding model prediction results for each of the six model types were extracted at these TF-
164 flexion angles. The 0° and 90° EOS reconstructions were not considered in the evaluation because
165 they were used for model calibrations, eliminating any model predictive capabilities. The root mean
166 square error (RMSE), mean differences with corresponding standard errors, Pearson's correlation
167 coefficient (R), coefficient of determination (R^2), and adjusted R^2 were calculated for each of the six
168 model predictions against the EOS experimental measures for each patellofemoral measure using
169 SPSS version 25.0 (SPSS, Chicago, IL, USA). The absolute values of R were then categorized as
170 weak, moderate, strong, or excellent prediction for $R \leq 0.35$, $0.35 < R \leq 0.67$, $0.67 < R \leq 0.90$, and

171 0.90 < R, accordingly[47]. The data was tested for normality using Shapiro-Wilk tests. Eighteen one-
172 way repeated measures ANOVAs (6 clinical measures at 3 lunge angles) were run with the necessary
173 Greenhouse-Geisser corrections. Due to the multiple comparisons and a small sample size, post-hoc
174 tests using Bonferroni adjustments ($\alpha = 0.05/18=0.002778$) were performed.

175 **3. Results**

176 Experimental and model subject means of each patellofemoral kinematic measure are depicted in
177 Figure 3, with standard deviations recorded in Supplementary Tables 2-8. Tables 1 and 2 display that
178 the lowest RMSE and mean differences for medial-lateral shift, superior-inferior translation, flexion-
179 extension, and patellar-rotation were achieved when utilizing a MA-PF joint, often decreasing with
180 added known tibiofemoral positions (MA, INT). However, utilizing a MA-PF with any tibiofemoral
181 joint type will result in underestimated tilt and AP translations. Additionally, the superior-Inferior (SI)
182 translation for high TF-flexion (60°) significantly overestimated the experimental data using a Hinge-
183 PF for all tibiofemoral models. Although the AP and tilt remain best predicted by a Hinge-PF with
184 MA-TF, the Int-TF with MA-PF decreases the mean differences in all measures besides SI. The
185 commonly used hinge model presented the most significantly different patellofemoral measures when
186 compared to the experimental EOS data especially in deep TF-flexion.

187 Overall, when using a MA-PF joint, the model predictive capabilities (R^2 , R^2 , and R_{adj}^2) increase for
188 ML, AP, SI, and patellar-rotation measures (Table 3); and furthermore, increase when modeling the
189 tibiofemoral with known positions (MA and INT models). Additionally, these measure all have strong
190 to excellent prediction capabilities. However, a MA-PF joint does not necessarily improve the PF-
191 flexion and tilt predictions, which both range in predictive capabilities from moderate to weak. PF-
192 flexion if best captured when modeling the tibiofemoral joint with known positions (MA and INT). In
193 general, the ML-shift, patellar-rotation and tilt are not well predicted by the models, with adjusted R^2
194 values ranging from 0.06 to 0.38 (Table 3).

195

196 **4. Discussion**

197 This study presents a novel way of modeling the patellofemoral joint, utilizing MRI and EOS
198 technology, and evaluates various models against in vivo kinematics extracted from consecutive
199 quasi-static lunge positions. The moving-axis model is derived from subject-specific bone
200 morphology and alignment. Being calibrated using two knee flexion positions (0° and 90°), the model
201 captures the true tibiofemoral and patellofemoral kinematics at these poses and estimates what occurs
202 in-between. Our results show that when changing a Hinge-PF to MA-PF joint provides more realistic
203 patellar motion in terms of ML-shift, SI-translation, and patellar-rotation, when compared to
204 experimental EOS. We found that AP translations are underestimated when using a MA-PF joint. This
205 could partially be explained by the strong correlation between posterior patellar translation and
206 posterior femoral translation [46] and the fact that our previously established tibiofemoral moving-
207 axis and hinge models resulted in significantly underestimated AP translations for all lunge conditions
208 [49].

209 Kinematics of the patella during dynamic weight-bearing [50] and unloaded [51,52] activities may not
210 be accurately predicted or represented from a passive supine position. Although bone geometries were
211 from lower limb MRI, the initial model positions were set to the EOS-0 configuration (weight-
212 bearing) to avoid these shortcomings. Patellofemoral kinematics can vary drastically between subjects
213 and throughout the knee flexion cycle. If future aims include determining optimal patient treatments
214 and or investigating injury progression it is important to consider subject-specific models that capture
215 more than just one time point based off anatomical landmarks selections.

216 Applying a moving-axis model to the patellofemoral joint has its limitations. Patella instability
217 normally occurs between 0° and 30° flexion. At this point, the patella may not be fully engaged with
218 the trochlear groove, and or beyond this flexion may not track in smooth patella motion [10,53]. There
219 is a chance that the patella was not sitting correctly in the trochlear groove during the EOS-0 scan. In
220 these cases, a piecewise linear relationship may not result in correct patellar motion. Furthermore, the
221 question of whether a linear relationship is appropriate for the MA-PF model is important to note;
222 perhaps a polynomial relationship would fit better, but this would require fitting the model to more
223 than two positions, like the INT-TF joint. In the future, evaluating other moving-axis relationships
224 against dynamic in vivo data, at more extreme ROM, may provide a more comprehensive validation.

225 Additionally, other computationally fast joint models should be considered such as a functional
226 patellofemoral hinge axis. Although a functional PF hinge axis may have given better results than our
227 cylinder fit hinge axis, we choose this for two main reasons: (1) it is known that for the tibiofemoral
228 joint the cylinder fit hinge axis is a better anatomical surrogate compared to a trans-epicondylar hinge
229 axis [54], we made the assumption that this would also hold true for the patellofemoral joint. (2) A
230 functional patellofemoral hinge axis would require two poses of the patella relative to the femur, and
231 many users may not have access to this kind of data. While creating a hinge joint by fitting cylinders to
232 scalable cadaver geometric data, similar to methods conducted in the Twente Lower Extremity Model
233 [21], may be a more manageable option.

234 In conclusion, we have successfully applied the concept of a moving-axis model to the patellofemoral
235 joint. The results show that a piecewise linear model can provide more accurate estimates of what is
236 going on in the patellofemoral joint between two active TF-flexion positions when compared to the
237 commonly used hinge joint. Most patellofemoral kinematics are best captured by using MA-PF with
238 an INT-TF joint, followed by a MA-TF and then Hinge-TF with MA-PF. In order to bring
239 musculoskeletal modeling of the patellofemoral joint to the clinical setting, the model needs to capture
240 more realistic joint kinematics (compared to the hinge) and be computationally fast (compared to the
241 existing multi-body contact models). While applying a moving-axis joint partially accomplishes this,
242 more investigation is needed to determine the best joint model for the clinical applications.

243

244 **Conflict of Interest**

245 Mark de Zee is co-founder of the company AnyBody Technology A/S, owning the AnyBody
246 Modeling System, which was used for the simulations. Mark de Zee is a minority shareholder on the
247 company. Christine Dzialo, is now an Anybody Technology employee. However, during her
248 participation in this project she was a PhD student under the supervision of Assoc. Prof. Michael
249 Skipper Andersen and had nothing to do with Anybody Technology apart from using their software.

250 **Acknowledgements**

251 This study was performed under the KNEEMO Initial Training Network, funded by the European
252 Union's Seventh Framework Programme for research, technological development, and demonstration
253 under Grant Agreement No. 607510 (www.kneemo.eu). This work was also supported by the Sapere
254 Aude program of the Danish Council for Independent Research under grant no. DFF-4184-00018 to
255 M. S. Andersen and the Innovation Fund Denmark under the Individualized Osteoarthritis
256 Intervention project.

257 **Ethical approval**

258 This study was approved by the Scientific Ethical Committee for the Region of Nordjylland and
259 informed consent was obtained prior to data collection.

260 J.nr.: 2016-000615

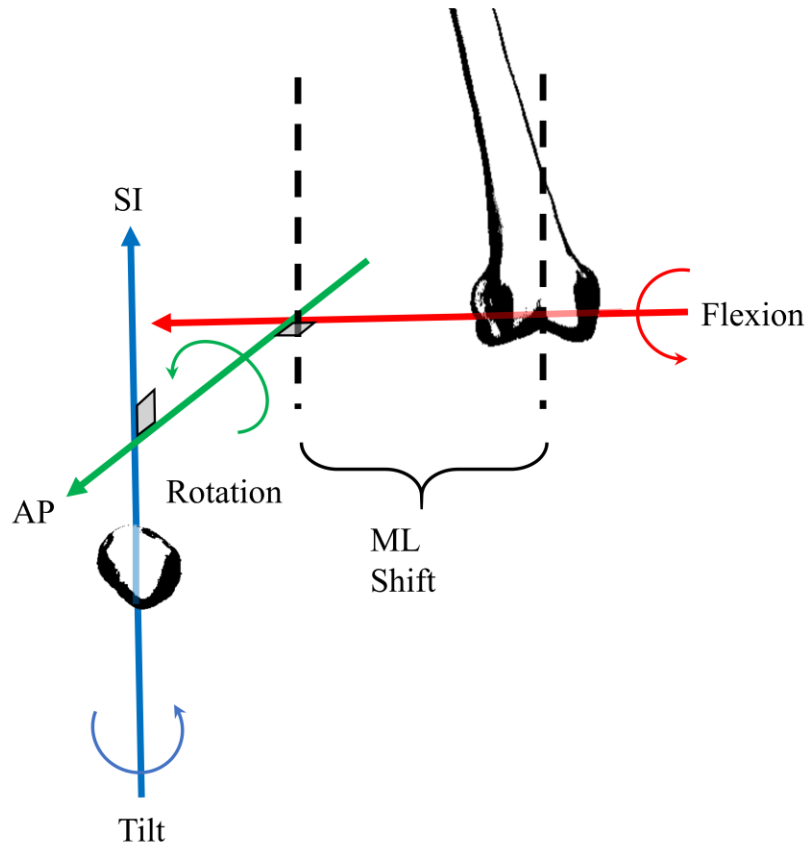
261 **References**

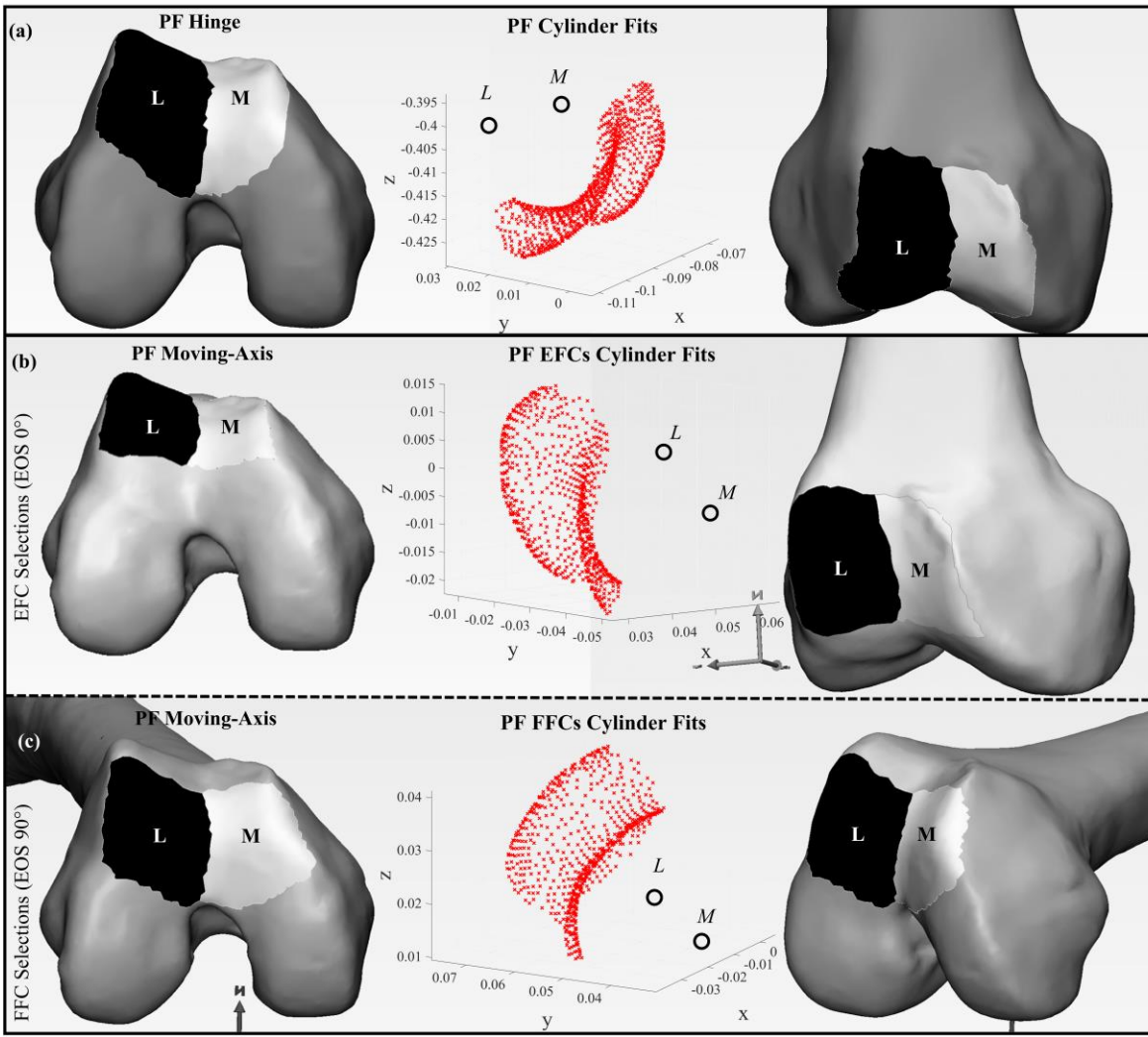
- 262 [1] Tecklenburg K, Dejour D, Hoser C, Fink C. Bony and cartilaginous anatomy of the
263 patellofemoral joint. *Knee Surgery, Sport Traumatol Arthrosc* 2006;14:235–40.
264 doi:10.1007/s00167-005-0683-0.
- 265 [2] Dye SF. Therapeutic implications of a tissue homeostasis approach to patellofemoral pain.
266 *Sports Med Arthrosc* 2001;9:206–311. doi:10.1097/00132585-200110000-00008.
- 267 [3] Dye SF. Patellofemoral pain current concepts: An overview. *Sports Med Arthrosc*
268 2001;9:264–72. doi:10.1097/00132585-200110000-00002.
- 269 [4] Witvrouw E, Werner S, Mikkelsen C, Van Tiggelen D, Vanden Berghe L, Cerulli G. Clinical
270 classification of patellofemoral pain syndrome: Guidelines for non-operative treatment. *Knee*
271 *Surgery, Sport Traumatol Arthrosc* 2005;13:122–30. doi:10.1007/s00167-004-0577-6.
- 272 [5] Crossley KM, Stefanik JJ, Selfe J, Collins NJ, Davis IS, Powers CM, et al. 2016
273 Patellofemoral pain consensus statement from the 4th International Patellofemoral Pain
274 Research Retreat, Manchester. Part 1: Terminology, definitions, clinical examination, natural
275 history, patellofemoral osteoarthritis and patient-reported outcome m. *Br J Sports Med*
276 2016;50:839–43. doi:10.1136/bjsports-2016-096384.
- 277 [6] Wittstein JR, Bartlett EC, Easterbrook J, Byrd JC. Magnetic Resonance Imaging Evaluation of
278 Patellofemoral Malalignment. *Arthroscopy* 2006;22:643–9. doi:10.1016/j.arthro.2006.03.005.
- 279 [7] Lankhorst NE, Bierma-Zeinstra SMA, van Middelkoop M. Factors associated with
280 patellofemoral pain syndrome: a systematic review. *Br J Sports Med* 2013;47:193–206.
281 doi:10.1136/bjsports-2011-090369.
- 282 [8] Wittstein JR, O'Brien SD, Vinson EN, Garrett WE. MRI evaluation of anterior knee pain:
283 Predicting response to nonoperative treatment. *Skeletal Radiol* 2009;38:895–901.
284 doi:10.1007/s00256-009-0698-6.

- 285 [9] Zhang LK, Wang XM, Niu YZ, Liu HX, Wang F. Relationship between Patellar Tracking and
286 the “Screw-home” Mechanism of Tibiofemoral Joint. *Orthop Surg* 2016;8:490–5.
287 doi:10.1111/os.12295.
- 288 [10] Waryasz GR, McDermott AY. Patellofemoral pain syndrome (PFPS): A systematic review of
289 anatomy and potential risk factors. *Dyn Med* 2008;7:1–14. doi:10.1186/1476-5918-7-9.
- 290 [11] Prins MR, van der Wurff P. Females with patellofemoral pain syndrome have weak hip
291 muscles: a systematic review. *Aust J Physiother* 2009;55:9–15. doi:10.1016/S0004-
292 9514(09)70055-8.
- 293 [12] Sheehan FT, Derasari A, Fine KM, Brindle TJ, Alter KE. Q-angle and J-sign: Indicative of
294 maltracking subgroups in patellofemoral pain. *Clin Orthop Relat Res* 2010;468:266–75.
295 doi:10.1007/s11999-009-0880-0.
- 296 [13] Moissenet F, Modenese L, Dumas R. Alterations of musculoskeletal models for a more
297 accurate estimation of lower limb joint contact forces during normal gait: A systematic review.
298 *J Biomech* 2017;63:8–20. doi:10.1016/j.jbiomech.2017.08.025.
- 299 [14] Sancisi N, Parenti-Castelli V. A New Kinematic Model of the Passive Motion of the Knee
300 Inclusive of the Patella. *J Mech Robot* 2011;3:041003. doi:10.1115/1.4004890.
- 301 [15] Lund ME, Andersen MS, Zee M De, Rasmussen J. Scaling of musculoskeletal models from
302 static and dynamic trials. *Int Biomech* 2015:37–41. doi:10.1080/23335432.2014.993706.
- 303 [16] Habachi A El, Moissenet F, Duprey S, Cheze L, Dumas R. Global sensitivity analysis of the
304 joint kinematics during gait to the parameters of a lower limb multi - body model. *Med Biol*
305 *Eng Comput* 2015:655–67. doi:10.1007/s11517-015-1269-8.
- 306 [17] Marra MA, Vanheule V, Fluit R, Koopman BHFJM, Rasmussen J, Verdonschot N, et al. A
307 Subject-Specific Musculoskeletal Modeling Framework to Predict In Vivo Mechanics of Total
308 Knee Arthroplasty. *J Biomech Eng* 2015;137:020904. doi:10.1115/1.4029258.
- 309 [18] Moissenet F, Chèze L, Dumas R. A 3D lower limb musculoskeletal model for simultaneous
310 estimation of musculo-tendon, joint contact, ligament and bone forces during gait. *J Biomech*
311 2014;47:50–8. doi:10.1016/j.jbiomech.2013.10.015.
- 312 [19] Thelen DG, Won Choi K, Schmitz AM. Co-simulation of neuromuscular dynamics and knee
313 mechanics during human walking. *J Biomech Eng* 2014;136:021033. doi:10.1115/1.4026358.
- 314 [20] Moissenet F, Chèze L, Dumas R. Influence of the Level of Muscular Redundancy on the
315 Validity of a Musculoskeletal Model. *J Biomech Eng* 2016;138:021019.
316 doi:10.1115/1.4032127.
- 317 [21] Carbone V, Fluit R, Pellikaan P, Krogt MM Van Der, Janssen D, Damsgaard M, et al. TLEM 2
318 . 0 – A comprehensive musculoskeletal geometry dataset for subject-specific modeling of
319 lower extremity 2015.
- 320 [22] Brito da Luz S, Modenese L, Sancisi N, Mills PM, Kennedy B, Beck BR, et al. Feasibility of
321 using MRIs to create subject-specific parallel-mechanism joint models. *J Biomech*
322 2017;53:45–55. doi:10.1016/j.jbiomech.2016.12.018.
- 323 [23] Marra MA, Strzelczak M, Heesterbeek PJC, van de Groes SAW, Janssen DW, Koopman
324 BFJM, et al. Anterior referencing of tibial slope in total knee arthroplasty considerably
325 influences knee kinematics: a musculoskeletal simulation study. *Knee Surgery, Sport*
326 *Traumatol Arthrosc* 2017:1–9. doi:10.1007/s00167-017-4561-3.
- 327 [24] Halonen KS, Dzialo CM, Mannisi M, Venäläinen MS, Zee M De, Andersen MS. Workflow

- 328 assessing the effect of gait alterations on stresses in the medial tibial cartilage – combined
 329 musculoskeletal modelling and finite element analysis. *Sci Rep* 2017;7:17396.
 330 doi:10.1038/s41598-017-17228-x.
- 331 [25] Smith CR, Vignos MF, Lenhart RL, Kaiser J. The Influence of Component Alignment and
 332 Ligament Properties on Tibiofemoral Contact Forces in Total Knee Replacement. *J Biomech*
 333 *Eng* 2017;138:021017:1-10. doi:10.1115/1.4032464.
- 334 [26] Guess TM, Stylianou AP, Kia M. Concurrent prediction of muscle and tibiofemoral contact
 335 forces during treadmill gait. *J Biomech Eng* 2014;136:021032:1-9. doi:10.1115/1.4026359.
- 336 [27] Hast MW, Piazza SJ. Dual-joint modeling for estimation of total knee replacement contact
 337 forces during locomotion. *J Biomech Eng* 2013;135:021013. doi:10.1115/1.4023320.
- 338 [28] Lenhart RL, Kaiser J, Smith CR, Thelen DG. Prediction and Validation of Load-Dependent
 339 Behavior of the Tibiofemoral and Patellofemoral Joints During Movement. *Ann Biomed Eng*
 340 2015;43:2675–85.
- 341 [29] Smith CR, Lenhart BSRL, Thelen DG, Kaiser J, Vignos MF. Influence of Ligament Properties
 342 on Tibiofemoral Mechanics in Walking. *J Knee Surgeryjournal Knee Surg* 2016;29:99–106.
- 343 [30] Walter JP, Kinney AL, Banks S a, D’Lima DD, Besier TF, Lloyd DG, et al. Muscle synergies
 344 may improve optimization prediction of knee contact forces during walking. *J Biomech Eng*
 345 2014;136:021031. doi:10.1115/1.4026428.
- 346 [31] Serrancolí G, Kinney AL, Fregly BJ, Font-Llagunes JM. Neuromusculoskeletal Model
 347 Calibration Significantly Affects Predicted Knee Contact Forces for Walking. *J Biomech Eng*
 348 2016;138:081001. doi:10.1115/1.4033673.
- 349 [32] Pedersen D, Vanheule V, Wirix-Speetjens R, Taylan O, Delpont HP, Scheys L, et al. A novel
 350 non-invasive method for measuring knee joint laxity in 6-DOF: in vitro proof-of-concept and
 351 validation. *J Biomech* 2018. doi:10.1016/j.jbiomech.2018.10.016.
- 352 [33] Dzialo CM, Pedersen Heide P, Simonsen CW, Krogh K, de Zee M, Andersen MS.
 353 Development and validation of subject-specific moving-axis tibiofemoral joint model using
 354 MRI and EOS imaging during a quasi-static lunge. *J Biomech* 2018.
 355 doi:10.1016/j.jbiomech.2018.02.032.
- 356 [34] Goh JC, Lee PY, Bose K, Goh JC. A cadaver study of the function of the oblique part of
 357 vastus medialis. *J Bone Jt Surgery Br Vol* 1995;77:225–31. doi:10.2106/00004623-
 358 199502000-00008.
- 359 [35] Bull AMJ, Katchburian M V., Shih YF, Amis AA. Standardisation of the description of
 360 patellofemoral motion and comparison between different techniques. *Knee Surgery, Sport*
 361 *Traumatol Arthrosc* 2002;10:184–93. doi:10.1007/s00167-001-0276-5.
- 362 [36] Kedgley AE, McWalter EJ, Wilson DR. The effect of coordinate system variation on in vivo
 363 patellofemoral kinematic measures. *Knee* 2015;22:88–94. doi:10.1016/j.knee.2014.11.006.
- 364 [37] Amis AA, Senavongse W, Bull AMJ. Patellofemoral Kinematics during Knee Flexion-
 365 Extension: An In Vitro Study. *J Orthop Res* 2006;2201–11.
- 366 [38] Grood ES, Suntay W. A Joint Coordinate System for the Clinical Description of Three-
 367 Dimensional Motions: Application to the Knee. *J Biomech Engineering* 1983;105:136–44.
- 368 [39] Hefzy MS, Jackson WT, Saddemi SR, Hsieh YF. Effects of tibial rotations on patellar tracking
 369 and patello-femoral contact areas. *J Biomed Eng* 1992;14:329–43. doi:10.1016/0141-
 370 5425(92)90008-9.

- 371 [40] Pennock GR, Clark KJ. An anatomy-based coordinate system for the description of the
372 kinematic displacements in the human knee. *J Biomech* 1990;23:1209–18. doi:10.1016/0021-
373 9290(90)90378-G.
- 374 [41] Suzuki T, Hosseini A, Li J-S, Gill TJ, Li G. In Vivo Patellar Tracking and Patellofemoral
375 Cartilage Contacts during Dynamic Stair Ascending Takashi. *J Biomech* 2012;45:2432–7.
376 doi:10.1016/j.jbiomech.2012.06.034.
- 377 [42] Churchill DL, Incavo SJ, Johnson CC, Beynnon BD. The transepicondylar axis approximates
378 the optimal flexion axis of the knee. *Clin Orthop Relat Res* 1998:111–8.
- 379 [43] Most E, Axe J, Rubash H, Li G. Sensitivity of the knee joint kinematics calculation to
380 selection of flexion axes. *J Biomech* 2004;37:1743–8. doi:10.1016/j.jbiomech.2004.01.025.
- 381 [44] Bowes MA, Vincent GR, Wolstenholme CB, Conaghan PG. A novel method for bone area
382 measurement provides new insights into osteoarthritis and its progression. *Ann Rheum Dis*
383 2015;74:519–25. doi:10.1136/annrheumdis-2013-204052.
- 384 [45] Drew BT, Bowes MA, Redmond AC, Dube B, Kingsbury SR, Conaghan PG. Patellofemoral
385 morphology is not related to pain using three-dimensional quantitative analysis in an older
386 population: data from the Osteoarthritis Initiative. *Rheumatology* 2017:2135–44.
387 doi:10.1093/rheumatology/kex329.
- 388 [46] Li G, Papannagari R, Nha KW, Defrate LE, Gill TJ, Rubash HE. The coupled motion of the
389 femur and patella during in vivo weightbearing knee flexion. *J Biomech Eng* 2007;129:937–
390 43. doi:10.1115/1.2803267.
- 391 [47] Taylor R. Interpretation of the Correlation Coefficient: A Basic Review. *J Diagnostic Med*
392 *Sonogr* 1990;1:35–9.
- 393 [48] Shull PB, Huang Y, Schlotman T, Reinbolt JA. Muscle force modification strategies are not
394 consistent for gait retraining to reduce the knee adduction moment in individuals with. *J*
395 *Biomech* 2015;48:3163–9. doi:10.1016/j.jbiomech.2015.07.006.
- 396 [49] Dzialo CM, Pedersen PH, Simonsen CW, Jensen KK, de Zee M, Andersen MS. Development
397 and validation of a subject-specific moving-axis tibiofemoral joint model using MRI and EOS
398 imaging during a quasi-static lunge. *J Biomech* 2018;72:71–80.
399 doi:10.1016/J.JBIOMECH.2018.02.032.
- 400 [50] Draper CE, Besier TF, Fredericson M, Santos JM, Beaupre GS, Delp SL, et al. Differences in
401 patellofemoral kinematics between weight-bearing and non-weight-bearing conditions in
402 patients with patellofemoral pain. *J Orthop Res* 2011;29:312–7. doi:10.1002/jor.21253.
- 403 [51] Freedman BR, Sheehan FT. Predicting Three-dimensional Patellofemoral Kinematics from
404 Static Imaging-Based Alignment Measures. *J Orthop Res* 2015;31:441–7.
405 doi:10.1002/jor.22246.
- 406 [52] D’Entremont AG, Nordmeyer-Massner JA, Bos C, Wilson DR, Pruessmann KP. Do dynamic-
407 based MR knee kinematics methods produce the same results as static methods? *Magn Reson*
408 *Med* 2013;69:1634–44. doi:10.1002/mrm.24425.
- 409 [53] Amis A. Current concept on anatomy and biomechanics of patellar stability. *Sport Med*
410 *Arthrosc Rev* 2007;15:48–56.
- 411 [54] Yin L, Chen K, Guo L, Cheng L, Wang F, Yang L. Identifying the functional flexion-
412 extension axis of the knee: An in-vivo kinematics study. *PLoS One* 2015;10:1–11.
413 doi:10.1371/journal.pone.0128877.





— TF(H)-PF(H) - - - TF(MA)-PF(H) - - - TF(H)-PF(MA) ··· TF(MA)-PF(MA) ★ EOS □ TF(Int)-PF(Hinge) ● TF(Int)-PF(MA)

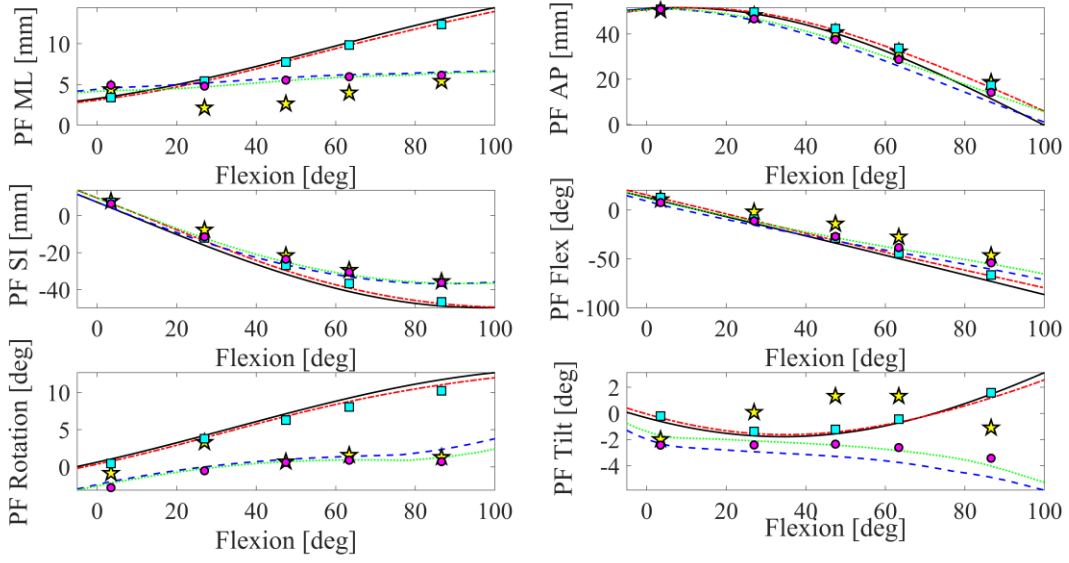


Figure 1—Description of patellar motion: **Medial-lateral shift** corresponds to the distance the patella origin moves along the fixed femoral axis (red), **Flexion** is defined as how much the patella rotates about the fixed femoral axis (red), **Anterior-posterior translation** corresponds to the distance the patella origin moves along the floating axis (green), **Rotation** is the amount the patella rotates about the floating axis (green), **Superior-inferior translation** corresponds to the distance traveled by the patella along the fixed patellar axis (blue), and **Tilt** is defined as the amount the patella rotates about the fixed patellar axis (blue). Image depicts directions of positive translations and rotations for right knee.

Figure 2—Patellofemoral contact surface selections and corresponding analytical surface fits on (a) EOS_0 Femur for hinge joint definition (b) EOS_0 Femur for extension facet center definition (c) and EOS_90 femur for flexion facet center definition. (b-c) are combined to define the moving-axis patellofemoral joint.

Figure 3—Subject mean data (n=10) of patellofemoral kinematic measures for the six model types and EOS data. *Standard deviations are listed in a Supplementary Tables 1-7 to avoid clutter and make for a clear image.*

Table 1—Root mean square error between experimental data (EOS) and various knee models for quasi-static lunge conditions **with respect to femur reference frame** for each clinical measure level for the given lunge conditions.

	Translations (mm)			Rotations (°)		
	ML	AP	SI	Flexion	Rotation	Tilt
<i>EOS - Hinge TF & PF</i>						
20° Flexion	4.54 ± 2.76	1.58 ± 1.33	7.44 ± 4.70	11.88 ± 7.55	4.26 ± 2.83	4.26 ± 5.57
45° Flexion	6.13 ± 3.43	3.99 ± 2.40	6.72 ± 3.76	19.81 ± 6.35	6.96 ± 3.21	6.21 ± 4.20
60° Flexion	6.70 ± 3.53	3.85 ± 2.80	9.30 ± 3.41	22.39 ± 7.38	8.75 ± 5.75	5.95 ± 4.08
Average	5.79 ± 1.88	3.14 ± 1.31	7.82 ± 2.30	18.03 ± 4.11	6.66 ± 2.39	5.47 ± 2.69
<i>EOS - Hinge TF : Moving-Axis PF</i>						
20° Flexion	3.77 ± 2.39	3.75 ± 1.67	5.50 ± 4.37	13.27 ± 10.66	5.45 ± 5.13	6.34 ± 6.13
45° Flexion	3.91 ± 3.33	7.03 ± 1.89	2.80 ± 1.92	16.73 ± 7.42	3.94 ± 2.68	7.08 ± 7.27
60° Flexion	2.65 ± 2.74	6.74 ± 2.76	1.81 ± 1.53	15.39 ± 7.54	4.03 ± 3.94	6.42 ± 6.07
Average	3.45 ± 1.64	5.84 ± 1.25	3.37 ± 1.67	15.13 ± 5.01	4.47 ± 2.33	6.61 ± 3.76
<i>EOS - Moving-Axis TF: Hinge PF</i>						
20° Flexion	4.32 ± 2.70	1.75 ± 1.07	5.29 ± 3.24	9.46 ± 6.41	4.16 ± 2.95	4.41 ± 5.47
45° Flexion	5.91 ± 3.34	2.52 ± 1.39	4.66 ± 2.84	16.61 ± 7.17	6.86 ± 3.01	5.78 ± 4.01
60° Flexion	6.47 ± 3.41	1.91 ± 1.35	7.46 ± 3.15	18.88 ± 8.23	8.72 ± 5.73	5.83 ± 3.99
Average	5.57 ± 1.83	2.06 ± 0.74	5.81 ± 1.78	14.98 ± 4.22	6.58 ± 2.37	5.34 ± 2.62
<i>EOS - Moving-Axis: TF & PF</i>						
20° Flexion	3.47 ± 2.38	3.13 ± 1.90	4.03 ± 2.71	10.46 ± 8.00	5.54 ± 5.68	5.94 ± 5.71
45° Flexion	3.64 ± 3.27	5.54 ± 1.44	1.82 ± 1.27	13.12 ± 6.00	4.17 ± 3.05	6.61 ± 6.45
60° Flexion	2.36 ± 2.67	4.61 ± 1.99	1.23 ± 0.94	11.65 ± 4.50	3.94 ± 4.71	5.84 ± 5.28
Average	3.16 ± 1.61	4.43 ± 1.03	2.36 ± 1.05	11.75 ± 3.66	4.55 ± 2.66	6.13 ± 3.37
<i>EOS - Interpolated TF : Hinge PF</i>						
20° Flexion	3.95 ± 2.51	2.00 ± 1.89	4.28 ± 2.48	7.79 ± 6.30	4.11 ± 3.27	4.59 ± 5.68
45° Flexion	5.63 ± 3.06	1.82 ± 1.96	5.24 ± 2.57	14.49 ± 7.42	7.01 ± 3.10	5.53 ± 4.33
60° Flexion	6.25 ± 3.29	2.01 ± 2.02	7.19 ± 3.21	16.75 ± 8.20	8.82 ± 5.59	5.73 ± 4.28
Average	5.28 ± 1.72	1.94 ± 1.13	5.57 ± 1.60	13.01 ± 4.24	6.65 ± 2.39	5.28 ± 2.78
<i>EOS - Interpolated TF : Moving-Axis PF</i>						
20° Flexion	3.29 ± 2.29	1.48 ± 1.41	3.83 ± 2.77	9.90 ± 8.11	5.38 ± 5.75	5.92 ± 5.29
45° Flexion	3.49 ± 3.19	3.10 ± 1.74	2.41 ± 1.92	12.86 ± 6.22	4.65 ± 2.92	6.59 ± 6.29
60° Flexion	2.35 ± 2.57	3.42 ± 2.23	1.52 ± 1.17	10.90 ± 4.90	4.08 ± 4.78	5.57 ± 5.10
Average	3.04 ± 1.56	2.67 ± 1.05	2.59 ± 1.19	11.22 ± 3.78	4.70 ± 2.68	6.03 ± 3.22

Table 2—Mean differences ± standard error between experimental data (EOS) and various knee models for quasi-static lunge conditions **with respect to femur reference frame**. Average (± SD) are calculated for each clinical measure. Symbol denotes that the clinical measure was statistically significantly different, appropriate Bonferroni adjustments were made for multiple comparisons, at $*(\alpha=0.05/18=0.002778)$ level for the given lunge condition.

	Translations (mm)			Rotations (°)		
	ML	AP	SI	Flexion	Rotation	Tilt
<i>EOS - Hinge TF & PF</i>						
20° Flexion	-3.95 ± 1.15	1.04 ± 0.58	7.44 ± 1.49	11.88 ± 2.39	-1.02 ± 1.64	1.35 ± 2.22
45° Flexion	-5.81 ± 1.26	3.86 ± 0.83	6.72 ± 1.19	19.81 ± 2.01*	-6.07 ± 1.53	2.01 ± 2.37
60° Flexion	-6.46 ± 1.26	3.35 ± 1.09	9.3 ± 1.08*	22.39 ± 2.33*	-7.03 ± 2.51	1.55 ± 2.31
Average	-5.41 ± 1.22	2.75 ± 0.83	7.82 ± 1.25	18.03 ± 2.24	-4.71 ± 1.89	1.64 ± 2.3
<i>EOS - Hinge TF : Moving-Axis PF</i>						
20° Flexion	-3.29 ± 0.97	3.75 ± 0.53*	5.16 ± 1.52	13.01 ± 3.48	3.71 ± 2.10	3.47 ± 2.62
45° Flexion	-3.36 ± 1.25	7.03 ± 0.60*	1.35 ± 1.02	16.73 ± 2.35*	0.03 ± 1.56	4.74 ± 2.89
60° Flexion	-2.36 ± 0.95	6.74 ± 0.87*	1.40 ± 0.62	15.39 ± 2.39*	0.32 ± 1.83	5.17 ± 2.30
Average	-3.01 ± 1.06	5.84 ± 0.67	2.63 ± 1.05	15.05 ± 2.74	1.35 ± 1.83	4.46 ± 2.61
<i>EOS - Moving-Axis TF: Hinge PF</i>						
20° Flexion	-3.70 ± 1.13	0.59 ± 0.65	5.29 ± 1.03	9.46 ± 2.03	-0.75 ± 1.65	1.14 ± 2.24
45° Flexion	-5.51 ± 1.27	2.2 ± 0.60	4.66 ± 0.90	16.61 ± 2.27*	-5.7 ± 1.59	1.91 ± 2.22
60° Flexion	-6.14 ± 1.27	0.84 ± 0.71	7.46 ± 10.00*	18.88 ± 2.60*	-6.61 ± 2.62	1.48 ± 2.26
Average	-5.12 ± 1.23	1.21 ± 0.65	5.81 ± 0.97	14.98 ± 2.30	-4.35 ± 1.95	1.51 ± 2.24

<i>EOS - Moving-Axis: TF & PF</i>						
20° Flexion	-2.91 ± 0.98	3.13 ± 0.60	3.26 ± 1.17	13.12 ± 2.77	3.97 ± 2.21	2.71 ± 2.52
45° Flexion	-3.05 ± 1.23	5.54 ± 0.45*	-0.16 ± 0.73	13.12 ± 1.90*	0.43 ± 1.69	3.99 ± 2.69
60° Flexion	-2.09 ± 0.92	4.61 ± 0.63*	0.28 ± 0.50	11.65 ± 1.42*	0.84 ± 0.50	4.41 ± 2.10
Average	-2.69 ± 1.04	4.43 ± 0.56	1.13 ± 0.80	12.63 ± 2.03	1.74 ± 1.46	3.7 ± 2.44
<i>EOS - Interpolated TF : Hinge PF</i>						
20° Flexion	-3.29 ± 1.08	-1.5 ± 0.74	4.28 ± 0.79	7.52 ± 2.11	-0.49 ± 1.71	1.46 ± 2.31
45° Flexion	-5.13 ± 1.24	-1.72 ± 0.65	5.24 ± 0.81*	14.49 ± 2.35	-5.59 ± 1.72	2.54 ± 2.13
60° Flexion	-5.88 ± 1.26	-1.56 ± 0.77	7.19 ± 1.02*	16.75 ± 2.59*	-6.48 ± 2.67	1.76 ± 2.26
Average	-4.76 ± 1.19	-1.59 ± 0.72	5.57 ± 0.87	12.92 ± 2.35	-4.19 ± 2.03	1.92 ± 2.24
<i>EOS - Interpolated TF : Moving-Axis PF</i>						
20° Flexion	-2.67 ± 0.96	1.48 ± 0.45	3.68 ± 0.94	9.24 ± 2.83	3.82 ± 2.22	2.5 ± 2.45
45° Flexion	-2.9 ± 1.2	3.1 ± 0.55	1.98 ± 0.76	12.86 ± 1.97*	0.08 ± 1.8	3.66 ± 2.7
60° Flexion	-1.98 ± 0.91	3.42 ± 0.71	1.04 ± 0.52	10.9 ± 1.55*	0.67 ± 2.02	3.93 ± 2.08
Average	-2.52 ± 1.03	2.67 ± 0.57	2.23 ± 0.74	11 ± 2.11	1.52 ± 2.01	3.36 ± 2.41

Table 3—Model predictive capabilities: Pearson’s Correlation Coefficient, coefficient of determination (R^2) and adjusted R^2 values calculated from model and experimental data (EOS) for quasi-static lunge angles (20°, 45°, 60°). R categorized as a weak (W) $r \leq 0.35$, moderate (M) $0.35 < r \leq 0.67$, strong (S) $0.67 < r \leq 0.90$, or excellent (E) $0.90 < r$ prediction.

	Model Compared with EOS	<i>Translations</i>			<i>Rotations</i>		
		ML	AP	SI	Flexion	Rotation	Tilt
R	Hinge: TF & PF	0.30 (W)	0.96 (E)	0.95 (E)	0.91 (E)	0.39 (M)	0.39 (M)
	Hinge TF : MA PF	0.57 (M)	0.98 (E)	0.97 (E)	0.81 (S)	0.48 (M)	0.30 (W)
	MA TF : Hinge PF	0.31 (W)	0.98 (E)	0.97 (E)	0.92 (E)	0.39 (M)	0.42 (M)
	MA: TF & PF	0.59 (M)	0.99 (E)	0.98 (E)	0.89 (S)	0.48 (M)	0.34 (W)
	Int. TF : Hinge PF	0.62 (M)	0.99 (E)	0.98 (E)	0.88 (S)	0.47 (M)	0.36 (M)
	Int. TF : MA PF	0.36 (M)	0.98 (E)	0.98 (E)	0.92 (E)	0.41 (M)	0.42 (M)
R^2	Hinge: TF & PF	0.09	0.93	0.90	0.83	0.15	0.15
	Hinge TF : MA PF	0.32	0.95	0.93	0.66	0.23	0.09
	MA TF : Hinge PF	0.10	0.96	0.94	0.85	0.15	0.17
	MA: TF & PF	0.35	0.98	0.96	0.80	0.23	0.11
	Int. TF : Hinge PF	0.13	0.96	0.95	0.85	0.17	0.17
	Int. TF : MA PF	0.39	0.99	0.97	0.78	0.22	0.13
R^2_{adj}	Hinge: TF & PF	0.06	0.93	0.90	0.83	0.12	0.12
	Hinge TF : MA PF	0.30	0.95	0.93	0.65	0.20	0.06
	MA TF : Hinge PF	0.07	0.96	0.94	0.85	0.12	0.14
	MA: TF & PF	0.33	0.98	0.95	0.79	0.21	0.08
	Int. TF : Hinge PF	0.10	0.96	0.95	0.85	0.14	0.14
	Int. TF : MA PF	0.36	0.99	0.97	0.77	0.19	0.10

Supplementary Table 1—Six different knee joint models with various combinations of tibiofemoral (TF) and patellofemoral (PF) joint types. A hinge joint axis can either defined between two anatomical landmarks or based on an analytical cylinder fit of a contact surface. A moving-axis (MA) joint articulates linearly between two known axes with respect to tibiofemoral flexion, these axes are derived from two known flexion positions and joint contact surface fits. We included one additional tibiofemoral joint model, Interpolation (INT), to isolate the patellofemoral model error by simulating the tibiofemoral positions and orientations of the five EOS reconstructions.

Model abbreviation	Tibiofemoral joint	Patellofemoral joint
<i>Hinge: TF-PF</i>	Hinge	Hinge
<i>Hinge TF : MA-PF</i>	Hinge	Moving-Axis
<i>MA-TF : Hinge-PF</i>	Moving-Axis	Hinge
<i>MA: TF-PF</i>	Moving-Axis	Moving-Axis
<i>INT-TF : Hinge-PF</i>	EOS Interpolation	Hinge
<i>INT-TF : MA-PF</i>	EOS Interpolation	Moving-Axis

Supplementary Table 2—Kinematic measures \pm standard deviation of the EOS in-vivo experimental data for quasi-static lunge conditions **with respect to femur reference frame**. Average (\pm SD) are calculated for each clinical measure.

Condition	Translations (mm)			Rotations ($^{\circ}$)		
	ML	AP	SI	Flexion	Rotation	Tilt
EOS_0	4.37 \pm 6.25	50.45 \pm 2.53	7.77 \pm 11.34	10.61 \pm 6.70	-0.85 \pm 5.24	-2.00 \pm 10.14
EOS_20	2.12 \pm 3.57	48.19 \pm 4.79	-7.76 \pm 10.34	-1.86 \pm 10.85	3.31 \pm 4.77	0.08 \pm 7.58
EOS_45	2.63 \pm 2.53	40.64 \pm 8.19	-21.58 \pm 10.56	-14.23 \pm 9.69	0.69 \pm 5.80	1.31 \pm 6.79
EOS_60	3.97 \pm 2.47	32.13 \pm 9.65	-29.48 \pm 7.22	-27.61 \pm 9.43	1.57 \pm 6.79	1.31 \pm 5.65
EOS_90	5.40 \pm 2.37	18.66 \pm 8.16	-35.58 \pm 5.06	-46.59 \pm 8.15	1.29 \pm 5.74	-1.11 \pm 5.52
Average (20-60)	2.91 \pm 2.86	40.32 \pm 7.54	-19.61 \pm 9.37	-14.57 \pm 9.99	1.86 \pm 5.79	0.90 \pm 6.68
Average (0-90)	3.70 \pm 3.44	38.01 \pm 6.66	-17.33 \pm 8.90	-15.94 \pm 8.97	1.20 \pm 5.67	-0.08 \pm 7.14
min	0.25 \pm 2.92	18.66 \pm 8.16	-35.58 \pm 5.06	-46.59 \pm 8.15	-2.83 \pm 6.04	-7.20 \pm 7.43
max	7.33 \pm 4.19	50.63 \pm 2.67	7.77 \pm 11.34	11.09 \pm 6.67	4.94 \pm 4.58	5.65 \pm 6.32
ROM	7.07 \pm 3.27	31.98 \pm 8.09	43.36 \pm 8.20	57.68 \pm 10.88	7.77 \pm 5.03	12.85 \pm 5.72

Supplementary Table 3—Kinematic measures \pm standard deviation of the **Hinge: TF-PF model** output for quasi-static lunge conditions **with respect to femur reference frame**. Average (\pm SD) are calculated for each clinical measure.

Condition	Translations (mm)			Translations (mm)		
	ML	AP	SI	Flexion	Rotation	Tilt
EOS_0	3.18 \pm 3.96	58.65 \pm 3.77	0.20 \pm 9.58	9.62 \pm 7.66	1.04 \pm 7.94	-1.92 \pm 5.28
EOS_20	6.08 \pm 3.14	47.14 \pm 5.30	-15.20 \pm 7.28	-13.75 \pm 9.25	4.32 \pm 6.40	-1.27 \pm 4.62
EOS_45	8.44 \pm 2.77	36.78 \pm 8.72	-28.30 \pm 8.36	-34.04 \pm 11.74	6.76 \pm 5.99	-0.70 \pm 5.91
EOS_60	10.43 \pm 3.74	28.78 \pm 9.43	-38.78 \pm 6.57	-50.00 \pm 13.79	8.60 \pm 5.52	-0.24 \pm 8.17
EOS_90	12.76 \pm 3.80	17.47 \pm 9.39	-54.51 \pm 5.28	-73.05 \pm 10.85	11.55 \pm 4.87	0.69 \pm 11.77
Average (20-60)	8.31 \pm 3.22	37.57 \pm 7.81	-27.43 \pm 7.40	-32.60 \pm 11.59	6.56 \pm 5.97	-0.74 \pm 6.23
Average (0-90)	8.18 \pm 3.48	37.76 \pm 7.32	-27.32 \pm 7.41	-32.24 \pm 10.66	6.46 \pm 6.14	-0.69 \pm 7.15
min	3.18 \pm 3.96	17.47 \pm 9.39	-54.51 \pm 5.28	-73.05 \pm 10.85	1.04 \pm 7.94	-6.07 \pm 5.89
max	12.76 \pm 3.80	58.65 \pm 3.77	0.20 \pm 9.58	9.62 \pm 7.66	11.55 \pm 4.87	4.84 \pm 8.32
ROM	9.59 \pm 4.85	41.18 \pm 9.71	54.71 \pm 10.41	82.68 \pm 13.26	10.51 \pm 6.94	10.91 \pm 8.94

Supplementary Table 4—Kinematic measures \pm standard deviation of the **Hinge TF: MA-PF model** output for quasi-static lunge conditions **with respect to femur reference frame**. Average (\pm SD) are calculated for each clinical measure.

Condition	Translations (mm)	Translations (mm)
-----------	-------------------	-------------------

	ML	AP	SI	Flexion	Rotation	Tilt
EOS_0	4.87 ± 5.96	56.47 ± 4.31	-1.06 ± 9.80	3.27 ± 10.31	-1.46 ± 8.45	-2.84 ± 9.01
EOS_20	5.42 ± 4.75	44.44 ± 6.03	-12.92 ± 7.43	-14.88 ± 7.67	-0.40 ± 6.98	-3.39 ± 7.61
EOS_45	5.99 ± 3.88	33.61 ± 8.69	-22.93 ± 8.79	-30.96 ± 7.23	0.66 ± 5.75	-3.43 ± 7.15
EOS_60	6.33 ± 3.34	25.38 ± 9.34	-30.88 ± 7.05	-43.01 ± 7.79	1.25 ± 4.91	-3.86 ± 7.10
EOS_90	6.47 ± 2.49	13.52 ± 8.60	-42.85 ± 4.92	-61.21 ± 8.45	2.37 ± 4.10	-3.61 ± 8.95
Average (20-60)	5.91 ± 3.99	34.48 ± 8.02	-22.24 ± 7.76	-29.62 ± 7.57	0.50 ± 5.88	-3.56 ± 7.29
Average (0-90)	5.82 ± 4.08	34.68 ± 7.39	-22.13 ± 7.60	-29.36 ± 8.29	0.48 ± 6.04	-3.43 ± 7.96
min	3.62 ± 3.91	13.52 ± 8.60	-42.85 ± 4.92	-61.21 ± 8.45	-2.28 ± 7.64	-7.65 ± 8.57
max	7.73 ± 4.30	56.47 ± 4.31	-1.06 ± 9.80	3.27 ± 10.31	3.19 ± 4.62	1.20 ± 6.69
ROM	4.10 ± 3.16	42.96 ± 8.94	41.80 ± 9.45	64.48 ± 13.76	5.47 ± 6.09	8.84 ± 6.62

Supplementary Table 5—Kinematic measures ± standard deviation of the **MA-TF: Hinge-PF model** output for quasi-static lunge conditions **with respect to femur reference frame**. Average (± SD) are calculated for each clinical measure.

Condition	Translations (mm)			Flexion	Translations (mm)	
	ML	AP	SI		Rotation	Tilt
EOS_0	2.96 ± 3.90	58.01 ± 3.67	2.58 ± 9.74	11.55 ± 7.24	0.85 ± 7.78	-1.61 ± 5.61
EOS_20	5.82 ± 3.10	47.60 ± 5.48	-13.05 ± 8.00	-11.32 ± 9.96	4.05 ± 6.46	-1.06 ± 4.71
EOS_45	8.14 ± 2.85	38.44 ± 8.78	-26.25 ± 9.29	-30.85 ± 13.04	6.40 ± 6.30	-0.60 ± 5.85
EOS_60	10.11 ± 3.87	31.29 ± 10.11	-36.95 ± 7.36	-46.49 ± 15.63	8.18 ± 6.06	-0.17 ± 8.06
EOS_90	12.37 ± 4.03	21.33 ± 10.36	-52.82 ± 5.89	-68.76 ± 13.56	11.02 ± 5.69	0.63 ± 11.56
Average (20-60)	8.02 ± 3.27	39.11 ± 8.13	-25.42 ± 8.22	-29.55 ± 12.88	6.21 ± 6.27	-0.61 ± 6.20
Average (0-90)	7.88 ± 3.55	39.33 ± 7.68	-25.30 ± 8.06	-29.17 ± 11.89	6.10 ± 6.46	-0.56 ± 7.16
min	2.96 ± 3.90	21.33 ± 10.36	-52.82 ± 5.89	-68.76 ± 13.56	0.85 ± 7.78	-5.95 ± 5.75
max	12.37 ± 4.03	58.01 ± 3.67	2.58 ± 9.74	11.55 ± 7.24	11.02 ± 5.69	4.96 ± 8.28
ROM	9.41 ± 5.21	36.68 ± 10.59	55.40 ± 10.52	80.31 ± 15.42	10.17 ± 6.58	10.91 ± 9.21

Supplementary Table 6—Kinematic measures ± standard deviation of the **MA: TF-PF model** output for quasi-static lunge conditions **with respect to femur reference frame**. Average (± SD) are calculated for each clinical measure.

Condition	Translations (mm)			Flexion	Translations (mm)	
	ML	AP	SI		Rotation	Tilt
EOS_0	4.47 ± 6.00	56.23 ± 3.94	1.28 ± 10.17	6.06 ± 8.77	-1.57 ± 8.73	-2.13 ± 8.84
EOS_20	5.04 ± 4.78	45.06 ± 6.30	-11.02 ± 8.23	-11.77 ± 7.60	-0.66 ± 7.53	-2.63 ± 7.21
EOS_45	5.68 ± 3.92	35.10 ± 9.21	-21.42 ± 9.72	-27.36 ± 8.27	0.27 ± 6.47	-2.68 ± 6.67
EOS_60	6.06 ± 3.41	27.52 ± 10.70	-29.77 ± 7.78	-39.27 ± 9.29	0.73 ± 5.76	-3.10 ± 6.43
EOS_90	6.22 ± 2.68	16.71 ± 10.55	-42.20 ± 5.26	-56.88 ± 9.61	1.70 ± 4.88	-2.80 ± 8.25
Average (20-60)	5.59 ± 4.03	35.89 ± 8.73	-20.74 ± 8.57	-26.13 ± 8.39	0.11 ± 6.59	-2.80 ± 6.77
Average (0-90)	5.49 ± 4.16	36.12 ± 8.14	-20.62 ± 8.23	-25.84 ± 8.71	0.09 ± 6.68	-2.67 ± 7.48
min	3.17 ± 3.95	16.71 ± 10.55	-42.20 ± 5.26	-56.88 ± 9.61	-2.36 ± 8.10	-6.95 ± 7.94
max	7.52 ± 4.34	56.23 ± 3.94	1.28 ± 10.17	6.06 ± 8.77	2.49 ± 5.24	2.02 ± 6.23
ROM	4.34 ± 3.35	39.52 ± 10.56	43.48 ± 8.91	62.94 ± 13.64	4.85 ± 5.23	8.97 ± 6.54

Supplementary Table 7—Kinematic measures ± standard deviation of the **INT-TF: Hinge-PF model** output for quasi-static lunge conditions **with respect to femur reference frame**. Average (± SD) are calculated for each clinical measure.

Condition	Translations (mm)			Translations (mm)		
	ML	AP	SI	Flexion	Rotation	Tilt
EOS_0	3.39 ± 3.86	50.91 ± 3.34	7.15 ± 8.95	12.73 ± 7.01	0.47 ± 6.39	-0.21 ± 5.65
EOS_20	5.42 ± 3.14	49.69 ± 4.78	-12.05 ± 9.29	-9.38 ± 10.51	3.79 ± 6.73	-1.38 ± 4.71
EOS_45	7.75 ± 2.91	42.36 ± 9.07	-26.82 ± 10.26	-28.72 ± 13.26	6.29 ± 7.16	-1.23 ± 5.71
EOS_60	9.84 ± 3.92	33.69 ± 11.39	-36.67 ± 6.94	-44.36 ± 15.60	8.05 ± 6.55	-0.44 ± 8.13
EOS_90	12.36 ± 4.19	17.28 ± 10.21	-46.58 ± 4.66	-66.50 ± 13.60	10.21 ± 4.42	1.58 ± 11.08
Average (20-60)	7.67 ± 3.33	41.91 ± 8.41	-25.18 ± 8.83	-27.49 ± 13.12	6.04 ± 6.82	-1.02 ± 6.18
Average (0-90)	7.75 ± 3.61	38.79 ± 7.76	-22.99 ± 8.02	-27.25 ± 12.00	5.76 ± 6.25	-0.34 ± 7.06
min	3.28 ± 3.57	17.28 ± 10.21	-46.58 ± 4.66	-66.50 ± 13.60	0.46 ± 6.39	-4.81 ± 5.70
max	12.36 ± 4.19	51.72 ± 3.34	7.15 ± 8.95	12.73 ± 7.01	10.73 ± 4.94	5.88 ± 7.99
ROM	9.08 ± 4.73	34.44 ± 9.59	53.73 ± 9.62	79.23 ± 15.03	10.27 ± 6.00	10.69 ± 8.31

Supplementary Table 8—Kinematic measures ± standard deviation of the **INT-TF: MA-PF model** output for quasi-static lunge conditions **with respect to femur reference frame**. Average (± SD) are calculated for each clinical measure.

Condition	Translations (mm)			Translations (mm)		
	ML	AP	SI	Flexion	Rotation	Tilt
EOS_0	4.92 ± 6.19	50.95 ± 3.24	6.43 ± 9.78	7.64 ± 8.27	-2.78 ± 8.59	-2.43 ± 9.42
EOS_20	4.80 ± 4.87	46.70 ± 5.78	-11.44 ± 8.97	-11.10 ± 8.09	-0.51 ± 7.45	-2.42 ± 7.20
EOS_45	5.53 ± 4.04	37.54 ± 9.60	-23.56 ± 9.76	-27.09 ± 8.03	0.62 ± 6.68	-2.36 ± 6.64
EOS_60	5.95 ± 3.37	28.71 ± 11.20	-30.52 ± 6.79	-38.51 ± 8.60	0.90 ± 6.12	-2.62 ± 6.59
EOS_90	6.13 ± 2.45	14.19 ± 9.32	-36.15 ± 4.98	-54.08 ± 9.01	0.71 ± 4.79	-3.43 ± 8.37
Average (20-60)	5.43 ± 4.09	37.65 ± 8.86	-21.84 ± 8.51	-25.57 ± 8.24	0.33 ± 6.75	-2.46 ± 6.81
Average (0-90)	5.47 ± 4.18	35.62 ± 7.83	-19.05 ± 8.06	-24.63 ± 8.40	-0.21 ± 6.73	-2.65 ± 7.64
min	2.98 ± 4.13	14.19 ± 9.32	-36.20 ± 4.93	-54.08 ± 9.01	-3.74 ± 7.87	-7.47 ± 8.50
max	7.76 ± 4.13	50.95 ± 3.24	6.43 ± 9.78	7.64 ± 8.27	2.48 ± 5.13	1.66 ± 6.18
ROM	4.78 ± 2.85	36.76 ± 9.66	42.64 ± 8.08	61.72 ± 13.17	6.22 ± 4.25	9.13 ± 5.95

Supplementary Table 9—ANOVA table for patellofemoral clinical measures taken from the origin of the patella anatomical coordinate system relative to the femoral anatomical coordinate system. *($\alpha=0.05/18=0.002778$) Bonferroni adjustments were made for multiple comparisons.

Clinical Measure	Lunge Angle	(I) model	(J) model	Mean Difference (I-J)	Std. Error	P-value	99.722% Confidence Interval for Differences	
							Lower Bound	Upper Bound
Lateral Shift (mm) ^a	20 ^b	EOS	TF (H)___PF (H)	-3.953	1.148	0.155	-11.250	3.344
		EOS	TF (H)___PF (MA)	-3.295	0.974	0.170	-9.485	2.896
		EOS	TF (MA)___PF (H)	-3.697	1.134	0.207	-10.902	3.509
		EOS	TF (MA)___PF (MA)	-2.912	0.981	0.331	-9.146	3.322
		EOS	TF (Int)___PF (H)	-3.290	1.078	0.289	-10.141	3.560
		EOS	TF (Int)___PF (MA)	-2.673	0.965	0.457	-8.804	3.458
	45 ^b	EOS	TF (H)___PF (H)	-5.811	1.263	0.027	-13.835	2.212
		EOS	TF (H)___PF (MA)	-3.363	1.246	0.514	-11.283	4.557
		EOS	TF (MA)___PF (H)	-5.510	1.272	0.040	-13.595	2.575
		EOS	TF (MA)___PF (MA)	-3.053	1.225	0.720	-10.839	4.732
		EOS	TF (Int)___PF (H)	-5.126	1.243	0.054	-13.021	2.770

		EOS	TF (Int)___PF (MA)	-2.903	1.199	0.808	-10.518	4.713
		EOS	TF (H)___PF (H)	-6.459	1.262	0.013	-14.479	1.562
		EOS	TF (H)___PF (MA)	-2.365	0.954	0.737	-8.427	3.698
	60 ^b	EOS	TF (MA)___PF (H)	-6.140	1.273	0.020	-14.228	1.948
		EOS	TF (MA)___PF (MA)	-2.093	0.918	1.000	-7.925	3.740
		EOS	TF (Int)___PF (H)	-5.876	1.258	0.025	-13.871	2.120
		EOS	TF (Int)___PF (MA)	-1.981	0.915	1.000	-7.793	3.831
		EOS	TF (H)___PF (H)	1.044	0.576	1.000	-2.618	4.706
		EOS	TF (H)___PF (MA)	3.748*	0.529	0.001	0.386	7.111
	20 ^b	EOS	TF (MA)___PF (H)	0.589	0.645	1.000	-3.510	4.689
		EOS	TF (MA)___PF (MA)	3.127	0.600	0.012	-0.687	6.941
		EOS	TF (Int)___PF (H)	-1.502	0.743	1.000	-6.225	3.222
		EOS	TF (Int)___PF (MA)	1.481	0.445	0.186	-1.349	4.312
		EOS	TF (H)___PF (H)	3.860	0.834	0.026	-1.437	9.157
		EOS	TF (H)___PF (MA)	7.031*	0.598	0.000	3.234	10.829
	45 ^b	EOS	TF (MA)___PF (H)	2.201	0.602	0.111	-1.626	6.028
		EOS	TF (MA)___PF (MA)	5.537*	0.455	0.000	2.648	8.426
		EOS	TF (Int)___PF (H)	-1.724	0.648	0.545	-5.840	2.391
		EOS	TF (Int)___PF (MA)	3.102	0.550	0.007	-0.394	6.598
		EOS	TF (H)___PF (H)	3.347	1.090	0.279	-3.576	10.271
		EOS	TF (H)___PF (MA)	6.744*	0.872	0.001	1.205	12.282
	60 ^b	EOS	TF (MA)___PF (H)	0.841	0.712	1.000	-3.686	5.368
		EOS	TF (MA)___PF (MA)	4.611*	0.630	0.001	0.610	8.612
		EOS	TF (Int)___PF (H)	-1.558	0.767	1.000	-6.429	3.314
		EOS	TF (Int)___PF (MA)	3.423	0.706	0.019	-1.062	7.908
		EOS	TF (H)___PF (H)	7.438	1.486	0.015	-2.002	16.879
		EOS	TF (H)___PF (MA)	5.157	1.522	0.169	-4.516	14.830
	20 ^b	EOS	TF (MA)___PF (H)	5.291	1.026	0.013	-1.228	11.809
		EOS	TF (MA)___PF (MA)	3.259	1.167	0.440	-4.155	10.673
		EOS	TF (Int)___PF (H)	4.284	0.785	0.008	-0.705	9.273
		EOS	TF (Int)___PF (MA)	3.681	0.944	0.076	-2.314	9.677
		EOS	TF (H)___PF (H)	6.721	1.188	0.007	-0.826	14.268
		EOS	TF (H)___PF (MA)	1.352	1.019	1.000	-5.122	7.825
	45 ^b	EOS	TF (MA)___PF (H)	4.664	0.898	0.012	-1.042	10.370
		EOS	TF (MA)___PF (MA)	-0.164	0.726	1.000	-4.776	4.448
		EOS	TF (Int)___PF (H)	5.236*	0.813	0.003	0.072	10.400
		EOS	TF (Int)___PF (MA)	1.979	0.761	0.604	-2.858	6.816
		EOS	TF (H)___PF (H)	9.297*	1.078	0.000	2.450	16.144
		EOS	TF (H)___PF (MA)	1.396	0.618	1.000	-2.528	5.320
	60 ^b	EOS	TF (MA)___PF (H)	7.463*	0.997	0.001	1.128	13.797
		EOS	TF (MA)___PF (MA)	0.283	0.497	1.000	-2.877	3.443
		EOS	TF (Int)___PF (H)	7.187*	1.017	0.001	0.728	13.646
		EOS	TF (Int)___PF (MA)	1.040	0.522	1.000	-2.275	4.356
		EOS	TF (H)___PF (H)	11.884	2.388	0.016	-3.286	27.054
		EOS	TF (H)___PF (MA)	13.013	3.478	0.097	-9.084	35.110
	20 ^b	EOS	TF (MA)___PF (H)	9.461	2.026	0.025	-3.413	22.334
		EOS	TF (MA)___PF (MA)	9.905	2.768	0.125	-7.684	27.495
		EOS	TF (Int)___PF (H)	7.520	2.106	0.126	-5.862	20.902
		EOS	TF (Int)___PF (MA)	9.239	2.827	0.204	-8.722	27.200
		EOS	TF (H)___PF (H)	19.807*	2.007	0.000	7.057	32.557
		EOS	TF (H)___PF (MA)	16.731*	2.347	0.001	1.816	31.647
	45 ^b	EOS	TF (MA)___PF (H)	16.612*	2.268	0.001	2.202	31.022
		EOS	TF (MA)___PF (MA)	13.123*	1.897	0.001	1.072	25.173
		EOS	TF (Int)___PF (H)	14.487	2.348	0.003	-0.429	29.403
		EOS	TF (Int)___PF (MA)	12.855*	1.967	0.002	0.360	25.351
		EOS	TF (H)___PF (H)	22.388*	2.335	0.000	7.554	37.222
	60 ^b	EOS	TF (H)___PF (MA)	15.394*	2.385	0.002	0.237	30.551
		EOS	TF (MA)___PF (H)	18.875*	2.603	0.001	2.334	35.416
		EOS	TF (MA)___PF (MA)	11.654*	1.424	0.000	2.604	20.704

		EOS	TF (Int)___PF (H)	16.752*	2.594	0.002	0.269	33.236
		EOS	TF (Int)___PF (MA)	10.897*	1.549	0.001	1.054	20.740
		EOS	TF (H)___PF (H)	-1.019	1.642	1.000	-11.455	9.417
		EOS	TF (H)___PF (MA)	3.706	2.099	1.000	-9.629	17.042
	20 ^b	EOS	TF (MA)___PF (H)	-0.748	1.652	1.000	-11.246	9.750
		EOS	TF (MA)___PF (MA)	3.967	2.210	1.000	-10.075	18.008
		EOS	TF (Int)___PF (H)	-0.487	1.707	1.000	-11.335	10.361
		EOS	TF (Int)___PF (MA)	3.819	2.216	1.000	-10.259	17.896
		EOS	TF (H)___PF (H)	-6.069	1.526	0.068	-15.765	3.626
		EOS	TF (H)___PF (MA)	0.032	1.562	1.000	-9.895	9.959
Patellar Rotation (deg) ^a	45 ^b	EOS	TF (MA)___PF (H)	-5.703	1.589	0.123	-15.798	4.392
		EOS	TF (MA)___PF (MA)	0.427	1.687	1.000	-10.290	11.145
		EOS	TF (Int)___PF (H)	-5.590	1.719	0.209	-16.512	5.331
		EOS	TF (Int)___PF (MA)	0.079	1.804	1.000	-11.385	11.543
		EOS	TF (H)___PF (H)	-7.030	2.515	0.438	-23.009	8.950
		EOS	TF (H)___PF (MA)	0.323	1.828	1.000	-11.291	11.938
	60 ^b	EOS	TF (MA)___PF (H)	-6.610	2.622	0.686	-23.267	10.046
		EOS	TF (MA)___PF (MA)	0.838	1.966	1.000	-11.655	13.332
		EOS	TF (Int)___PF (H)	-6.481	2.666	0.796	-23.418	10.457
		EOS	TF (Int)___PF (MA)	0.672	2.021	1.000	-12.170	13.515
		EOS	TF (H)___PF (H)	1.349	2.216	1.000	-12.731	15.429
		EOS	TF (H)___PF (MA)	3.469	2.625	1.000	-13.209	20.147
	20 ^b	EOS	TF (MA)___PF (H)	1.142	2.236	1.000	-13.068	15.351
		EOS	TF (MA)___PF (MA)	2.709	2.524	1.000	-13.326	18.745
		EOS	TF (Int)___PF (H)	1.463	2.309	1.000	-13.208	16.135
		EOS	TF (Int)___PF (MA)	2.497	2.449	1.000	-13.061	18.054
		EOS	TF (H)___PF (H)	2.011	2.367	1.000	-13.029	17.051
		EOS	TF (H)___PF (MA)	4.742	2.892	1.000	-13.633	23.117
Patellar Tilt (deg) ^a	45 ^b	EOS	TF (MA)___PF (H)	1.912	2.216	1.000	-12.169	15.994
		EOS	TF (MA)___PF (MA)	3.986	2.693	1.000	-13.122	21.095
		EOS	TF (Int)___PF (H)	2.542	2.134	1.000	-11.018	16.101
		EOS	TF (Int)___PF (MA)	3.665	2.701	1.000	-13.494	20.824
		EOS	TF (H)___PF (H)	1.549	2.307	1.000	-13.112	16.210
		EOS	TF (H)___PF (MA)	5.167	2.301	1.000	-9.453	19.787
	60 ^b	EOS	TF (MA)___PF (H)	1.485	2.263	1.000	-12.895	15.864
		EOS	TF (MA)___PF (MA)	4.409	2.100	1.000	-8.935	17.753
		EOS	TF (Int)___PF (H)	1.756	2.265	1.000	-12.635	16.147
		EOS	TF (Int)___PF (MA)	3.930	2.079	1.000	-9.282	17.142